The International Journal of Advanced Manufacturing Technology (2020) 106:5241–5254
https://doi.org/10.1007/s00170-020-05014-5

ORIGINAL ARTICLE

Mechanical and cutting performance of cemented carbide tools with Cr/*x*/DLC composite coatings

Tianmei Hao[1] · Jin Du[1] · Guosheng Su[1] · Peirong Zhang[1] · Yujing Sun[1] · Jingjie Zhang[1]

Received: 23 September 2019 / Accepted: 27 January 2020 / Published online: 5February 2020
© Springer-Verlag London Ltd., part of Springer Nature 2020

Abstract

Diamond-like carbon (DLC)-coated tools are suitable for the machining of various aluminum alloys, graphite, and other non-ferrous metals. The shortcomings of DLC-coated tools such as high internal residual stress, low toughness, and poor adhesion strength limit their application. In order to reveal the mechanical and cutting performance of DLC-coated tools, a DLC monolayer coating, Cr/CrN/DLC composite coating, and Cr/W-DLC/DLC composite coating had been prepared on the cemented carbide cutting tools. The influences of transition interlayer on the microstructure and mechanical properties of DLC coatings were analyzed. Tool lives, wear mechanism, and machined surface roughness obtained with uncoated cemented carbide tool, DLC monolayer–coated tool, and Cr/*x*/DLC-coated tool during the machining of Al-Si alloys were investigated. Compared with DLC monolayer coating, the strength ratio (ID/IG) of the DLC composite coatings with Cr/*x* transition structure was improved, while the sp^3 covalent bond contents was decreased. The results show that the adhesion strength and toughness of the Cr/*x*/DLC composite coating were enhanced, and the residual stress was greatly reduced. The cutting tests further indicate that the DLC coating significantly improved the tool life. Based on comprehensive evaluation, the Cr/W-DLC/DLC composite coating has the highest adhesion, highest toughness, the lowest residual stress, and the longest tool life, and it is suitable for the machining of non-ferrous metal.

Keywords DLC · Composite coating · Cemented carbide · Mechanical properties · Tool life

1 Introduction

Diamond-like carbon (DLC) film is a metastable amorphous material formed by the combination of sp^1, sp^2, and sp^3 covalent bonds coordinating carbon atoms, and a C–H covalent bond is present in the hydrogen-containing DLC. The sp^2 and sp^3 covalent bonds represent graphite structure and diamond structure, respectively. According to the $sp^2/(sp^2 + sp^3)$ ratio and hydrogen content in DLC, the DLC is divided into four categories: tetrahedral carbon film (tα-C, sp^3 covalent bond content is higher than 80%), hydrogenated tetrahedral carbon film (α:C–H, sp^3 covalent bond content is higher than 70%), hydrogen-free amorphous carbon film (α-C), and amorphous diamond film (α-D) [1]. DLC coatings can be prepared through different deposition techniques, including physical vapor deposition (PVD), chemical vapor deposition (CVD), and liquid phase electro-deposition [2]. DLC coating exhibits low surface roughness, high hardness, low friction coefficient, strong wear, and corrosion resistance, and can be deposited on the cutting tools, molds, bearings, seal rings, and other key components. The research about DLC coating is an important development direction in the field of high hardness and wear-resisting coating in the future [3]. At present, DLC coatings have been widely used in metal cutting, such as turning, milling, and drilling of non-ferrous alloys, as shown in Table 1 [4–12]. However, the DLC coating also has disadvantages such as high internal residual stress, low toughness, and poor adhesion, which limits its further application especially in the machining of difficult-to-cut materials [13].

Unremitting efforts have been committed to investigate the mechanical properties of DLC, so as to improve its adhesion with substrate and decrease its residual stress. The commonly methods to alleviate the residual stress and enhance its adhesion are doping, adding transition interlayer, setting bias,

✉ Jin Du
dj84105@126.com

[1] School of Mechanical and Automotive Engineering, Qilu University of Technology (Shandong Academy of Sciences), Jinan 250353, Shandong, China

Table 1 Research status on machining with DLC-coated tools

Machining method	Coating and substrate	Workpiece	Preparation technology	Coating thickness	Performance	Key remarks	Refs
Turning	Ti-C:H; CrC/Cr/DLC; Ti-DLC/α-C:H and cemented carbide tools	Ti6Al4V alloy; Al–Si alloys; glass fiber reinforced.	PACVD; mid-frequency reactive magnetron sputtering/linear ion source technology	1–2.5 μm	Compressive stress; hardness; Elastic modulus; adhesion; toughness; friction coefficient; flank wear; Wear form; machined surface roughness.	→ DLC-coated tools had higher hardness and elastic modulus, it could reduce machining forces and release internal stress. → Multilayer coated tools had the best adhesion, toughness, friction properties, minimum wear rate and longest service life. → Multilayer coated tools had best machined surface quality, and the abrasive wear is the primary wear form.	[4–6]
Milling	DLC and cemented carbide; ultra-fine carbide tools	Inconel 718; AlMg2.5 alloy; AlCu4.5Si12 alloy.	PACVD; vacuum arc discharge	0.2–1.2 μm	Tool wear; built-up edge and burr; cutting force; machined surface roughness; curl diameter; cutting tool lives.	→ DLC-coated tools had less built-up edge and less burrs with long distance. → DLC-coated tools had smaller cutting forces and preferable wear resistance. → DLC-coated tools had lower roughness values of machined surfaces and smaller chip curl diameter.	[7, 8]
Drilling	H-DLC; ta-C; NH-DLC and cemented carbide drills, HSS drill	Cast Al-Si alloys; CFRP and AA7075; 319 grade cast aluminum alloy.	PACVD; PVD	1-5 μm	Failure criterion; built-up edge; tool life; hole quality; chip type; undersurface morphology; thrust forces; torque.	→ H-DLC-coated drills prolonged the tool life and can substitute the use of CVD diamond–coated tools. → The H-DLC had advantages over the NH-DLC grade coatings in keeping the cutting forces low and limiting adhesion. → Ta-C has better combination of characteristics and more suitable for drilling.	[9–12]

annealing, and so on. Some studies have shown that the doping and biasing methods are effective for reducing residual stress; however, the hardness and elastic modulus of DLC are also weakened, and the surface roughness of the coating is also greatly increased [5, 14]. The annealing treatment can maintain the high hardness of DLC while reducing the internal residual stress. However, many substrate materials cannot withstand the high temperature of 773–873 K, and the annealing treatment changes the coating structure and deteriorates the thermal stability in practice [15, 16]. Therefore, the application of annealing aim to promote the mechanical properties of DLC is limited. It has been found that the addition transition interlayers between the substrate material and the DLC coating is one of the most effective method to solve the mismatch between the coating and the substrate [17]. The roles of transition interlayer not only improve the DLC adhesion but also reduce the internal residual stress by narrowing the difference in thermal expansion coefficient, crystal structure, and chemical composition mismatch between the interfaces. The complex interface structure formed by the addition of transition interlayers enhances the interfacial material's hindrance to dislocation slip and to inhibit the formation and propagation of cracks, thus improves the toughness and deformation resistance of the DLC coating [18]. In addition, due to the high solubility and high diffusion coefficient of C in Co, the Co element in cemented carbide is not conducive to the nucleation of C atoms, and has a catalytic effect on the formation of soft graphite phase [19]. Therefore, the addition of transition interlayers performs an important role in the DLC coating on the cemented carbide substrate which contains Co element. Huang et al. [6] deposited Ti-DLC/DLC multilayer coating on cemented carbide substrate, the results shown that the adhesion and toughness of the multilayer coating were better than DLC monolayer coating; moreover, the friction coefficient and wear rate of the DLC multilayers were significantly lower than that of a DLC monolayer coating.

Cast Al-Si alloy (AC9B), belonging to hypereutectic (Si > 13 wt%) structure, has the advantages of low density and favorable strength to weight ratio. It is widely used in aerospace, automotive, and instrumentation industries. However, the Al-Si alloy (AC9B) has poor machinability, and the small chips generated during the cutting process may scratch the machined surface which lead to poor surface quality and serious tool wear. The traditional coatings like TiC, TiN, Al_2O_3, and AlN have limitations in the cutting of Al–Si alloy. On the one hand, the traditional coatings showed rapid wear due to strong adhesion and chemical reaction with Al-Si alloys [19]. On the other hand, the hard silicon phase in the alloys can lead to severe hard particle wear and even breakage during the machining, which makes it difficult to obtain machining accuracy and reduce tool service life [4]. In contrast, DLC-coated tools have perfectly chemical inertness and inherently self-lubricating properties, and are appropriate for the cutting of Al-Si alloys. Giovanni et al. [4, 7] prepared DLC coating on the surface of cemented carbide tools and found that the performance of DLC-coated tools was better than that of uncoated tools, which not only reduces the surface roughness of the machined surface but also reduces the cutting forces by approximately 50%, meanwhile it could extend tool life.

Considering the potential application of DLC composite–coated tools in cutting Al-Si alloys, DLC monolayer coating and DLC composite coatings with Cr/*x* transition interlayers (Cr/CrN/DLC and Cr/W-DLC/DLC composite coatings) were prepared in this investigation. In the preparation process of composite coating, the transition interlayers (Cr, CrN, W-DLC) were added between the YG8-cemented carbide substrate and DLC coating. The influence of transition interlayers structure on the mechanical properties of DLC coating was comprehensively analyzed. The effect of different transition interlayers on the adhesion properties and internal residual stress of DLC composite coating structure was discussed. Finally, the effect of the transition interlayers on the cutting performance of DLC-coated tools was investigated by the cutting Al-Si alloys test, which provides the theoretical basis and technical support for the preparing of DLC-coated tools with good comprehensive properties.

1.1 Experimental procedure

1.1.1 Deposition principle of DLC composite coating

Three transition interlayers (transition metals (Cr) interlayer, metal compounds (CrN) interlayer, and W element–doped interlayer) are designed to have a coefficient of thermal expansion similar to that of YG8 (WC 92%, Co 8%)-cemented carbide substrate and DLC coating, and can also be used for hardness transitions. As a transition element, Cr has higher hardness, higher density, good ductility and conductivity, and thermal conductivity. Depositing a proper thickness of Cr layer on the interface can form an effective bonding interface and improve the adhesion of the film [20]. Designing a Cr/*x* multilayer film can hinder the growth of the Cr layer's columnar crystals and refine the crystal grains. The second transition interlayers of the two composite coatings are CrN and W-DLC. The performance of W-DLC is closer to that of DLC coating. The hardness and wear resistance of the CrN transition interlayer coating are lower than that of the W-DLC transition interlayer [21, 22]. HauTer Coater (HC-1500) coating equipment was employed to prepare Cr/CrN/DLC, Cr/W-DLC/DLC, and DLC using sequential deposition method. The preparation principle is that the substrate periodically exposes to independent DC magnetron sputtering deposition sources and plasma-assisted chemical deposition source. The equipment controls the deposition period and then controls the film's thickness, as shown in Fig. 1. It is equipped with a vacuum chamber for two orthogonally mounted plasma

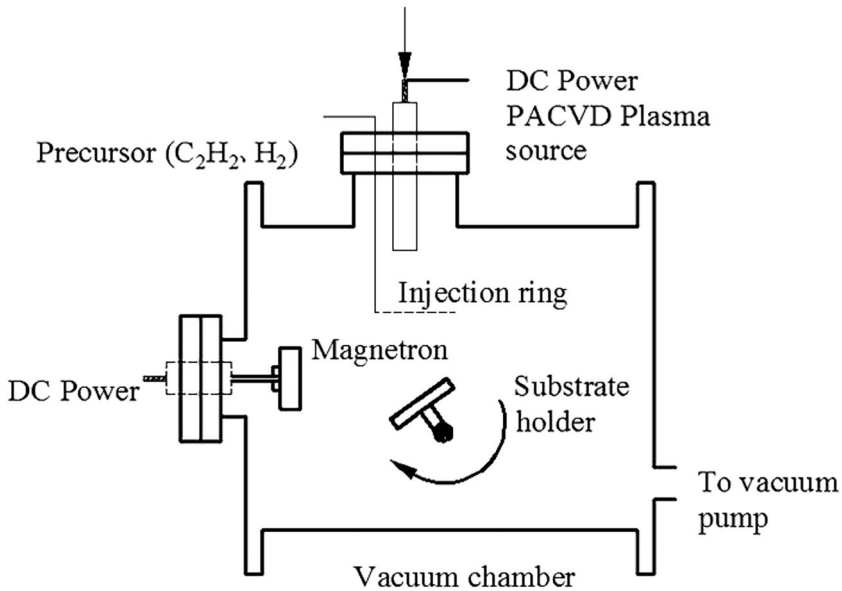

Fig. 1 Schematic of the sequential deposition system

sources: a magnetron for Cr, CrN deposition; a WC target for W-DLC deposition; and a PACVD plasma source for DLC deposition from argon and acetylene mixture. The substrate was transported between the two plasma sources by a stepper motor. Primary pump and turbo molecular pump were used for evacuation. Then argon glow discharges in order to etch and clean the substrate to remove large particles of impurities and oxidized contaminants on the surface, and improve the surface roughness of the substrate to form an adhesion favorable condition for the transition interlayers. Under the bias setting, acetylene precipitates carbon ions and bombards the substrate, thus deposits a diamond-like carbon film on the surface of the substrate. Detailed deposition parameters were exhibited in Table 2.The thicknesses of three coatings were Cr/CrN/DLC-2.7 μm, Cr/W-DLC/DLC-3.3 μm, and a monolayer DLC-1.8 μm, respectively.

Table 2 Deposition parameters for the coatings

Cr/CrN interlayer	Magnetron
W-DLC interlayer	WC target
DLC layer	Mixture of Ar/C_2H_2
Deposition temperature (K)	< 473
Sputtering power (W)	1000–3000
Ion beam source (V)	1000–1500
Ar flow rate (sccm)	5
C_2H_2 flow rate (sccm)	70
Gas pressure (Pa)	2.7
Bias power (V)	1000–2000
Duty cycle	20–60%
Vacuum pressure (Pa)	5×10^{-2}

1.2 Microstructure and mechanical properties of DLC coating

Variations of carbon hybrid bond and amorphous crystal structure were probed use Raman spectroscopy (laser wavelength of 514.5 nm, Ar + laser power of 50 mw). The cross-sectional morphology and element distribution observation of the coating were measured use a laser scanning electron microscope (SEM) and X-ray energy spectroscopy (EDS). The hardness and elasticity modulus of Cr/CrN/DLC, Cr /W-DLC/DLC multilayer coatings and DLC monolayer coating were tested using a Nanoidentation Tester with Oliver-Pharr measurement method [23] with a load of 20 mN. The coating adhesion was obtained by scratch test using the Revetest Scratch Tester (RST). During the scratch test, the diamond indenter type was AJ-290 with a radius of 200 μm and the linear loading method was applied with a scratch length of 3 mm.

1.3 Cutting performance of DLC-coated tools

Several cutting tests were carried out to investigate the cutting performance of DLC-coated tools in the machining of cast Al-Si alloy AC9B. YG8 (size 13 mm × 13 mm × 4.5 mm)-cemented carbide tools were singled out as the substrate with rank angle γ_0 of 20°, clearance angle α_0 of 0°, and inclination angle λ_s of 0°. All of the cutting tests were carried out on a general lathe CA6140 (maximum speed 1400 r/min, power

Table 3 Chemical composition of Cast Al-Si alloy (AC9B) (wt%)

Element	Si	Cu	Fe	Mn	Mg	Ni	Ti	Zn	Al
Content	19.68	0.55	0.65	0.13	1.01	1.00	0.15	0.07	76.77

Table 4 Machining parameters and conditions

Workpiece	Al–19.68%Si alloy (140 mm dia. × 300-mm-long cast bar)
Tool substrate	Zcc 41305A
Tool holder	MSBNR2525M12
Cutting speed (v_c)	150 m/min
Radial cutting depth(a_p)	0.4 mm
Rutting feed rate (f)	0.1 mm/rev
Cutting condition	Dry

7.5 kW). The workpiece (AC9B alloy) was subjected to solution treatment at 783.15 K for 2 h and quenching at 483.15 K for 7 h. The Brinell hardness of the AC9B aluminum silicon alloy after heating treatment was 110. The elemental composition of the workpiece was determined through X-ray energy spectroscopy (EDS) and the measured results are displayed in Table 3, which meets the composition requirements of the literature [24]. The cutting test belongs to a single factor test to investigate the effect of cutting speed on the cutting performance under the dry cutting conditions. Machining parameters and conditions are shown in Table 4. After the cutting tests, the flank wear of the cutting tools were measured by microscopic observation and the cutting tool lives were recorded. The roughness of the machined surfaces after machining was measured using a handheld roughness meter (TIME TR200). The description of the experiment methodology flow chart is shown in Fig. 2.

2 Results and discussion

2.1 Microstructure of DLC coating

Figure 3 shows the cross-sectional morphology of uncoated tools. It can be seen from Fig. 3 that there are fewer surface defects, the grain structure is plump-eared, and the grain morphology is mainly quadrilateral structure of WC. Moreover, the grains are uniformly distributed with high density and lower porosity, which conforms to the typical grain morphology of cemented carbide [25]. Cross-sectional morphology of DLC composite coating with transition interlayers on YG8-cemented carbide substrate were observed as shown in Fig. 4a, b, and c. A typical transition interlayer structure can be clearly observed from Fig. 4. The coatings grow homogeneously, with there appears no defects like pinholes and droplet. The boundaries of the gradient transition interlayers are

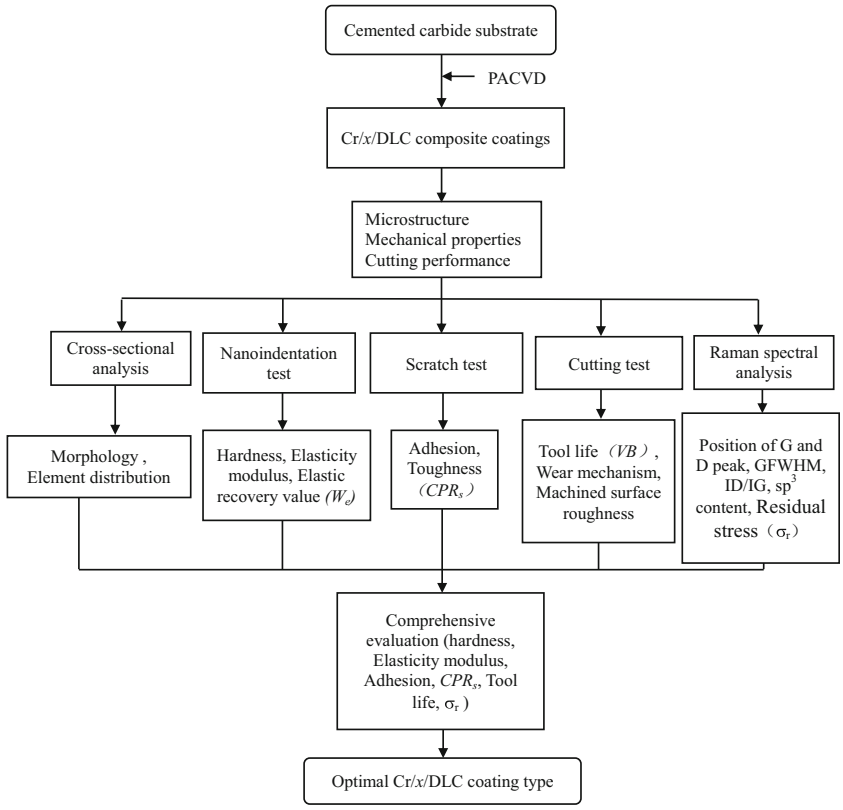

Fig. 2 Flow chart of the experiment methodology

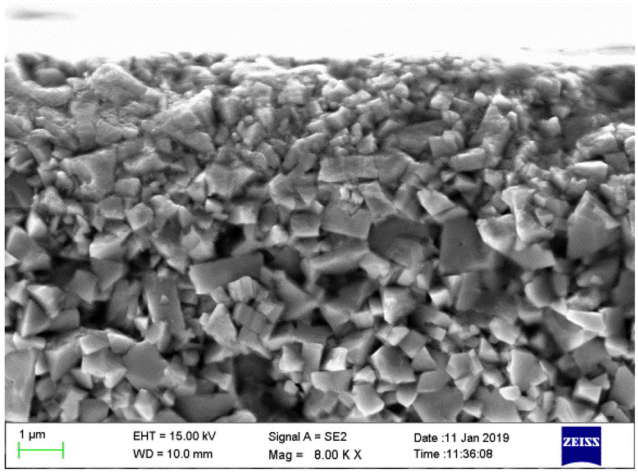

Fig. 3 Cross-sectional morphology of uncoated tools

tightly combined without obvious delamination or peeling, which indicates the microstructure of the DLC, Cr/CrN/DLC, and Cr/W-DLC/DLC composite coatings was fine. The EDS spectral line scanning area is indicated by the arrowed line in the cross-sectional morphology of Fig. 4a, b, and c, and the arrow direction indicates the EDS spectrum line scanning direction.

Figure 4d, e, and f show the elements line distribution for the three coatings of DLC, Cr/CrN/DLC, and Cr/W-DLC/DLC, respectively. Since the substrate is YG8 belongs to the W-Co-type cemented carbide, so there is a large amount of W element and Co element that are contained in the EDS spectral line scan substrate region. From Fig.4d, it can be seen that there contain three elements, W, Co, and C, because the outermost layer of the coating is a DLC coating, so the content of C element in the coating area is significantly increased. In Fig. 4e, it can be observed that in addition to the W and Co elements, there are also Cr and C elements, and the N element content is small since it belongs to the category of light elements. Combined with the SEM test results, it can be clearly seen that the composite coating has obvious boundaries with other coating or substrate, and the distribution of elements confirms that the prepared composite coating is Cr/CrN/DLC composite coating. In Fig. 4f, in addition to the substrate

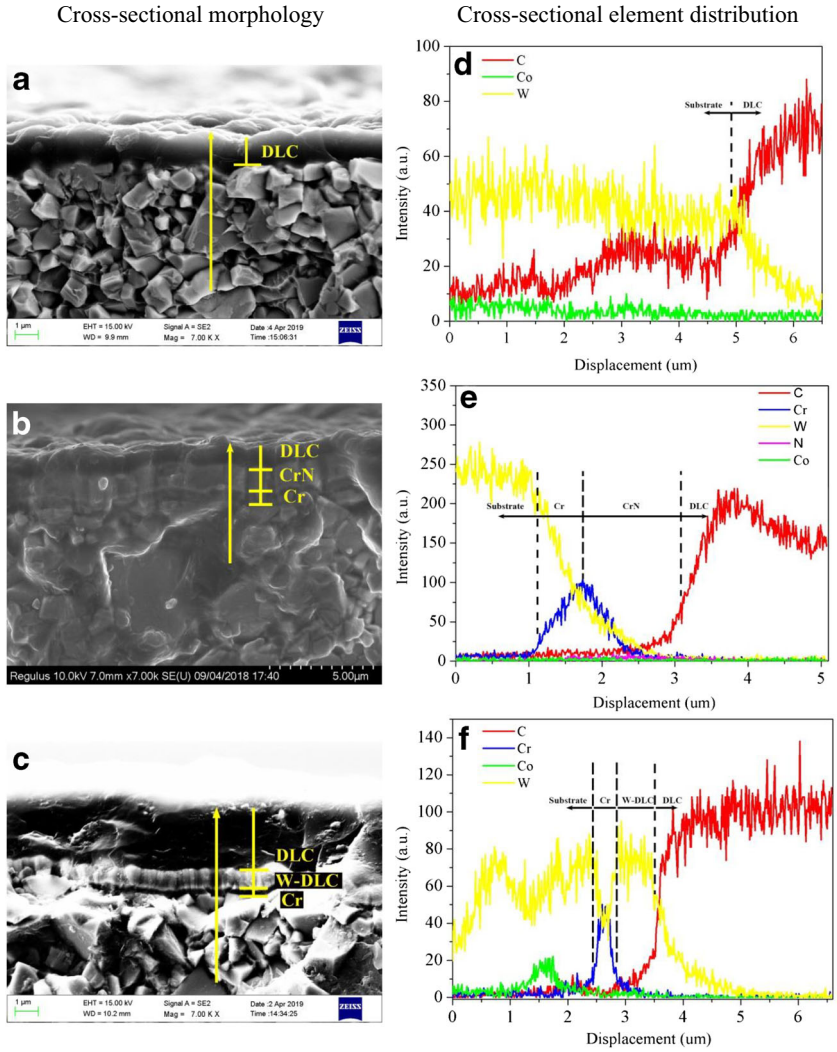

Fig. 4 Cross-sectional morphology and element distribution of coated tools: **a**, **d** DLC monolayer coating; **b**, **e** Cr/CrN/DLC composite coating; and **c**, **f** Cr/W-DLC/DLC composite coating

elements W and Co, the coating region also contains Cr, W, and C elements. It can be obviously seen that the content of each element in the Cr/W-DLC/DLC composite coating is apparently distributed. It is confirmed that Fig. 4c is a Cr/W-DLC/DLC composite coating.

The Gaussian deconvoluted Raman spectra for DLC, Cr/CrN/DLC, and Cr/W-DLC/DLC coatings are represent in Fig. 5. According to Raman spectra fitting results, the G and D peak positions of the three coatings are located at around of 1350 to 1580 cm^{-1}, which conform to the typical asymmetric oblique scattering amorphous carbon structure [26].

As can be seen from Figs. 6 and 7, compared with DLC monolayer coating, the full width at half maximum of G peak (GFWHM) of DLC composite coating with transition interlayers increased from 102.93 to 113.97 and 115.38, and the same as a comparatively high intensity ratio of D peak to G peak (ID/IG). The value of ID/IG increases from 1.19 to 1.25

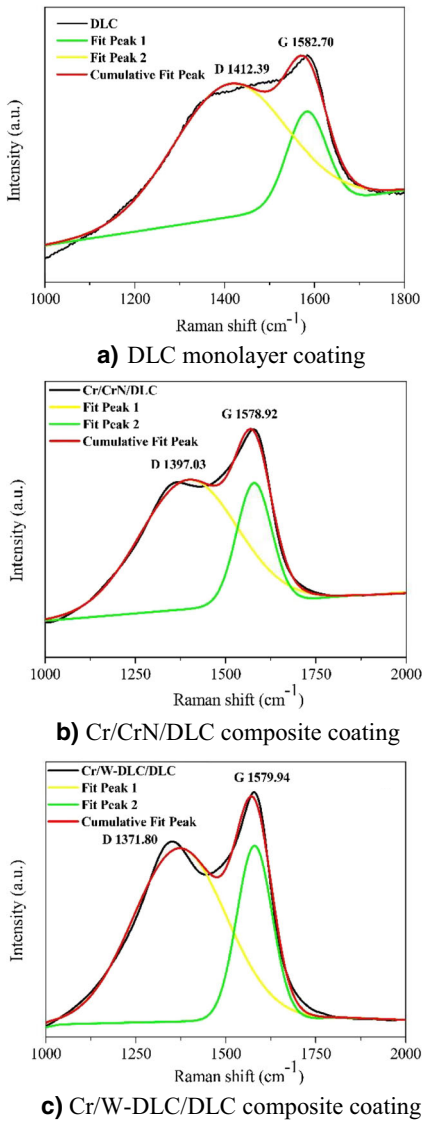

Fig. 5 Raman spectra of DLC coatings

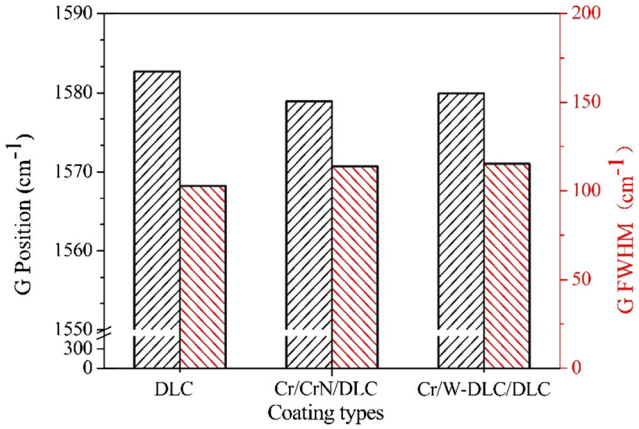

Fig. 6 Relationship between the FWHM of the G band and the G peak position

and 1.28, while the content of sp^3 covalent bond decreases from 0.80 to 0.67 and 0.69. The full width at half maximum of G peak (GFWHM) can indicate the properties of the sample. If the properties are relatively single, the full width at half maximum of G peak (GFWHM) is narrow and the peak spectrum becomes sharp. On the contrary, the full width at half maximum of G peak (GFWHM) is wide and the peak spectrum is slow. This also indicates that the DLC monolayer coating has single properties. Related literature reports [27–29] that the ID/IG value reflects the structural order of the coating, which is proportional to the number and size of sp^2 clusters in the film. This indicates that after adding the transition interlayers, the multilayer coating has a better structural order and reduces the sp^3 covalent bond content in the outermost DLC film, meanwhile increasing the sp^2 bond content. And then, the structure of DLC coating with different Cr/*x* transition interlayers tends to be graphite and the hardness decreased. Furthermore, in the gradient transition model, the compressive stress is the key to the formation of sp^3 covalent bond structure [5]. It can be further deducted that the adding Cr/*x* transition interlayers has the ability to reduce the internal

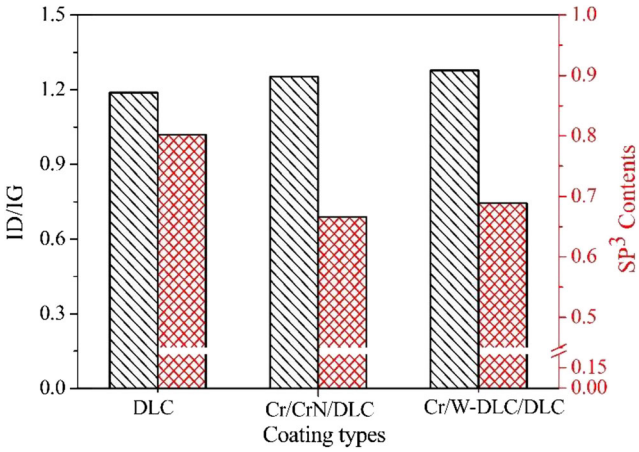

Fig. 7 ID/IG Ratio and the sp^3 covalent bond contents

residual stress through reducing the covalent bond content of sp^3 (C–C).

2.2 Mechanical properties of DLC coating

The high-energy ion bombardment and the interface mismatch between coating and substrate during the deposition of DLC coating lead to internal tensile stress or compressive stress. In order to calculate and compare the residual stress in the coatings, the following equation was employed [30]:

$$\sigma_r = -565.6\frac{\omega-\omega_0}{\omega_0} \quad (1)$$

where σ_r is the residual stress (GPa), ω is the G peak position of the coating (cm^{-1}), and ω_0 is the G peak position of the pure graphite. According to Eq. (1), the relationship of residual stress between three different coatings is calculated shown in Fig. 8. The DLC monolayer coating had the highest residual stress of 0.97 GPa. The residual stress of the DLC composite coating containing Cr/CrN transition interlayers drops to 0.38 GPa. The residual stress of the DLC composite coating containing Cr/W-DLC transition interlayer drops to 0.02 GPa. From the calculation results of residual stress, it can be concluded that the two transition interfaces are contributed to release the internal residual stress in the DLC coating. As the case of carbon-based films, high sp^3 covalent bond content tends to result in high hardness and high internal stress [5]. Combined with the results of Raman spectrum analysis, the reason for the reduction of residual stress in the transition interlayers is the increase of sp^2 covalent bond contents. The Raman characteristic peak of a DLC monolayer coating was shifted to the right while the internal stress was high, which is also consistent with the view of Sahoo. Sahoo et al. [19] considered that the reason for the Raman spectrum positive shift was the higher stress and the distortion of crystal structure. In addition, there is slipping or dislocation in the transition interlayers structure of Cr, CrN, and W-DLC. The lipping or dislocation between interlayers can absorb plastic deformation,

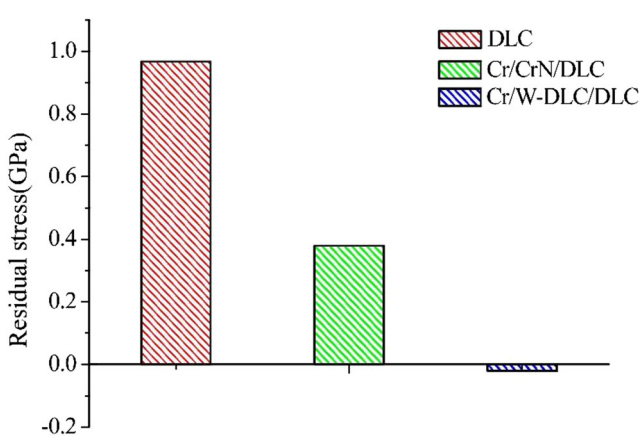

Fig. 8 Internal residual stress of different DLC coatings

which helps to release the internal stress.

The hardness and elastic modulus of these three coatings are measured by nanoindentation, and the results are shown in Fig. 9. The hardness of Cr/CrN/DLC and Cr/W-DLC/DLC composite coating was 15.43 GPa and 18.86 GPa, respectively, while the DLC monolayer coating was 20.50 GPa. The elastic modulus manifests a similar variation trend that Cr/CrN/DLC, Cr/W-DLC/DLC composite coatings were 168.17 GPa and 180.50 GPa while the monolayer DLC coating was 258.76 GPa. This is consistent with the test prediction for hardness in the Raman spectra test analysis, and reaffirms that the sp^3 covalent bond content can enhance the hardness of DLC coatings. It had also shown that the transition interlayers could reduce the hardness and elastic modulus, due to the reduction of sp^3 covalent bond content and the increase of graphite phase [27]. Thus, the Cr/*x* transition interlayers can be reduced in hardness by reducing the content of the sp^3 covalent bond, and the low hardness of the DLC composite coating having the transition interlayers is due to the relatively low hardness of Cr and CrN intermediate layers.

The elastic recovery value (W_e) originated from the typical load–displacement curves, which are shown in Fig. 10. The W_e value shows the elasticity recovery capacity, and it can better characterize the toughness of the specimen to some degree [27]. The elastic recovery value (W_e) used the following equation:

$$[(h_{max}-h_r)/h_{max}] \times 100\% \quad (2)$$

where h_{max} is the maximum indentation depth during loading and h_r is the residual indentation depth after unloading. For the composite coating, the W_e level of the Cr/CrN/DLC and Cr/W-DLC/DLC coating was 38.10% and 41.82%, respectively. The W_e value of the DLC monolayer coating decreases to 31.74% compared with the DLC composite coating. This reflects the elastic or reversible deformation is conspicuous during the indentation experimentation. The elastic recovery ability of the DLC composite coating with different Cr/*x* transition interlayer structures was better than that of the DLC monolayer coating, and the Cr/W-DLC/DLC composite coating had the best elastic recovery ability.

The adhesion and toughness for the three coatings tested under scratch tests are presented in Fig. 11. Adhesion strength is affected by the composition and structure of the coating as well as by the thickness of the coating, the hardness of the substrate, and the friction coefficient between the coating and the indenter. The main difference between Cr/CrN/DLC and Cr/W-DLC/DLC composite coatings is the intermediate layers, but the adhesion strength had a considerable difference. The Cr/W-DLC/DLC coating had the highest adhesion of 116.56 GPa, which was on account of the dense coating structure deposited by PACVD technique and the inherent characteristics of the transition metal carbide (WC) interlayer. Nevertheless, the

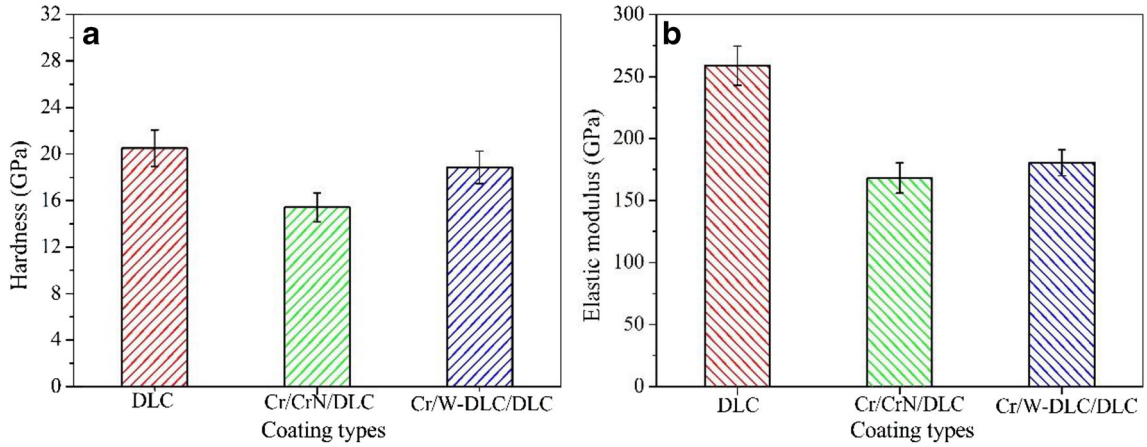

Fig. 9 **a** Hardness of the coating. **b** Elasticity modulus of the coating

adhesion of the Cr/CrN/DLC composite coatings was 73.18 GPa that is much lower than the Cr/W-DLC/DLC. The monolayer DLC coating had the lowest adhesion of 69.68 N. This can be attributed to two reasons: first, the existence of the transition interlayers makes the elastic modulus between the adjacent films more similar. The residual stress between the interfaces created a gradient mode with the intermediate hard layer deposition. The gradient residual stress reduces the resistance between the individual layers, which greatly increase the adhesion and provide greater support for the coating structure. Second, slight multi-phase mixed growth is formed at the interface during the growth of the thin films, which will weaken the slippage and separation between the layers.

The coating fracture toughness reflects the ability of absorbing plastic deformation work and fracture work during the process from deformation to fracture. The coating toughness in this study is represented through scratch crack propagation resistance (CPR_s) [31], expressed as follows:

$$CPR_s = L_{c1}(L_{c2} - L_{c1}) \quad (3)$$

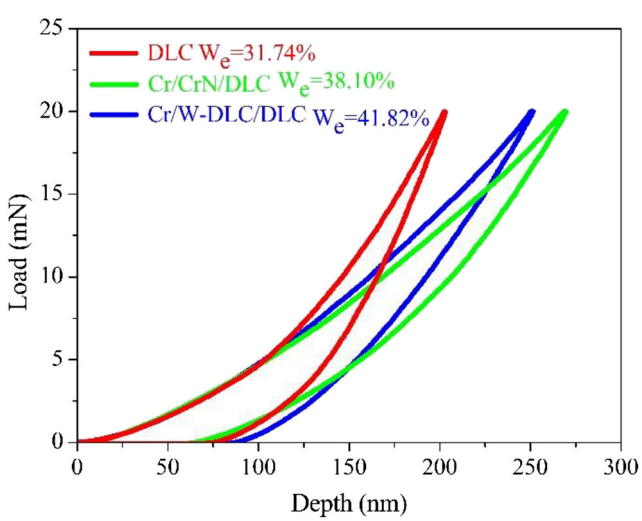

Fig. 10 Typical load–displacement curves during indentation test

where the L_{c1} indicates the initial peeling point load. L_{c2} stands for the critical load which indicating the occurrence of delamination and adhesion failure of the coating [6]. Figure 12 is a scratched morphology of three coatings. The micrographs corresponding to L_{c1} and L_{c2} have been shown in the two wireframes in Fig. 12, where a, c, and e represent L_{c1}, and b, d, and f represent L_{c2}. The Cr/CrN/DLC and Cr/W-DLC/DLC composite coating's toughness was 1290 N^2 and 1712 N^2, separately. However, the DLC monolayer coating's toughness much lower than two the previous composite coatings was 1169 N^2. In addition, the results of coating's toughness characterized by scratch crack propagation resistance (CPR_s) were consistent with the trend of toughness reflected by the elastic recovery value (W_e) in the above indentation test, which confirms that the toughness of the composite coatings is improved by introducing the transition interlayers. According to the research [32], the decrease of sp^3 covalent bond content in a composite coating could result in a comparatively low hardness, but contributed to an increase in coating's toughness. This explains the cause of toughness change from the perspective

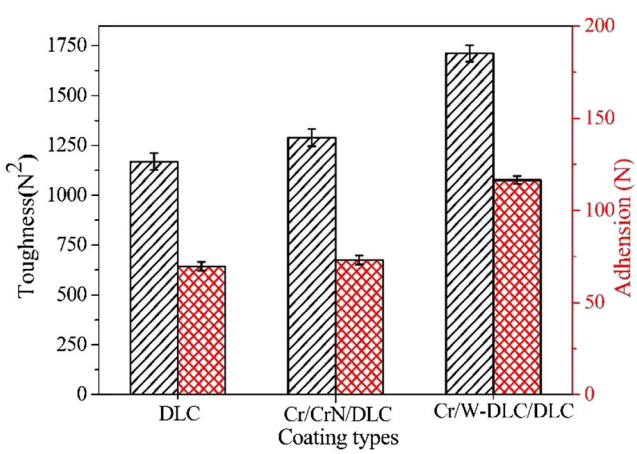

Fig. 11 Adhesion and toughness of DLC coatings

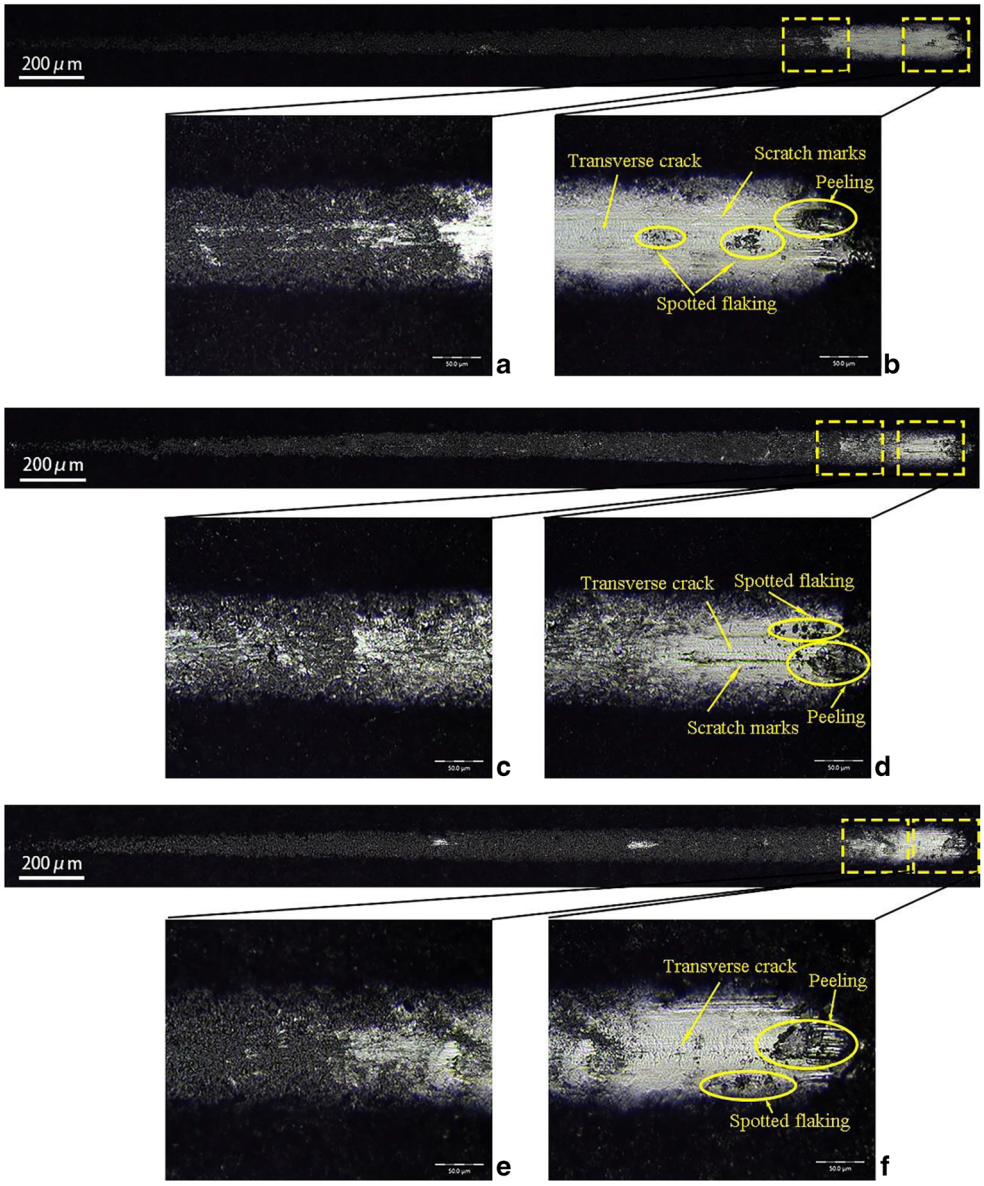

Fig. 12 Scratch morphology: **a**, **b** DLC coating, **c**, **d** Cr/CrN/DLC composite coating, and **e**, **f** Cr/W-DLC/DLC composite coating

of a chemical bond perspective. The failure morphology of the three coatings can be clearly observed form Fig. 12b, d, and f. Some slight scratch marks and slight transverse cracks are clearly seen in the middle of the scratch of a DLC monolayer coating. Large area peeling is seen in the central region and obvious scratch marks and a small amount of spotted flaking at the end of scratch are observed from Cr/CrN/DLC composite coatings. Some transverse cracks and a small amount of spotted flaking at the scratch edges are observed in Cr/W-DLC/DLC composite coating. The Cr/CrN/DLC and Cr/W-DLC/DLC composite coatings exhibit sufficient adhesion strength and scratch crack propagation resistance due to the interfacial effect of the transition interlayer. The interfacial effect of the transition interlayers inhibits crack propagation [33]. This is attributed to the energy dissipation and crack deflection caused by the transition interlayer, thus improving the toughness and adhesion of the DLC composite coatings.

2.3 Cutting performance of DLC-coated tools

Figure 13 indicates the flank wear of uncoated and DLC-coated cemented carbide tools as a function of machining distance. The wear morphology of tool flank was observed by microscope and the tool flank wear (VB) was measured. In this work, VB = 0.3 mm was recognized as the blunt criterion of cutting tools. As can be seen from Fig. 13, the uncoated tool exhibits a comparatively higher wear rate during the machining. The cutting life of uncoated tool was about 4600 m. The flank wear of DLC-coated tools rapidly increases to about 0.15 mm at the machining distance of 1600 m, and then slowly rising for a long cutting distance afterwards. Cr/CrN/DLC-

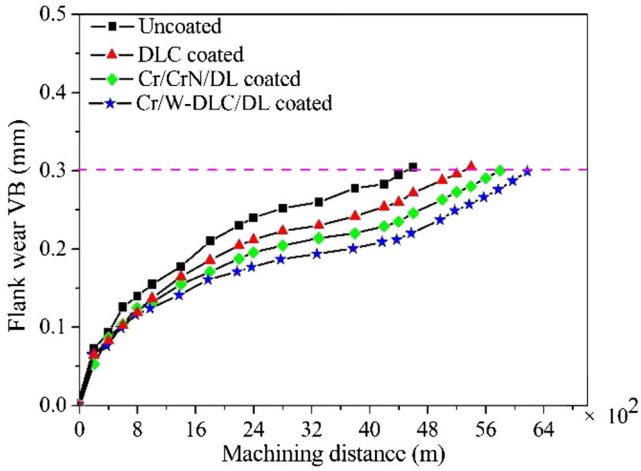

Fig. 13 Tool life of uncoated and DLC-coated tools. **a** DLC-coated tool. **b** Cr/CrN/DLC-coated tool. **c** Cr/W-DLC/DLC-coated tool. **d** Uncoated cemented carbide tool

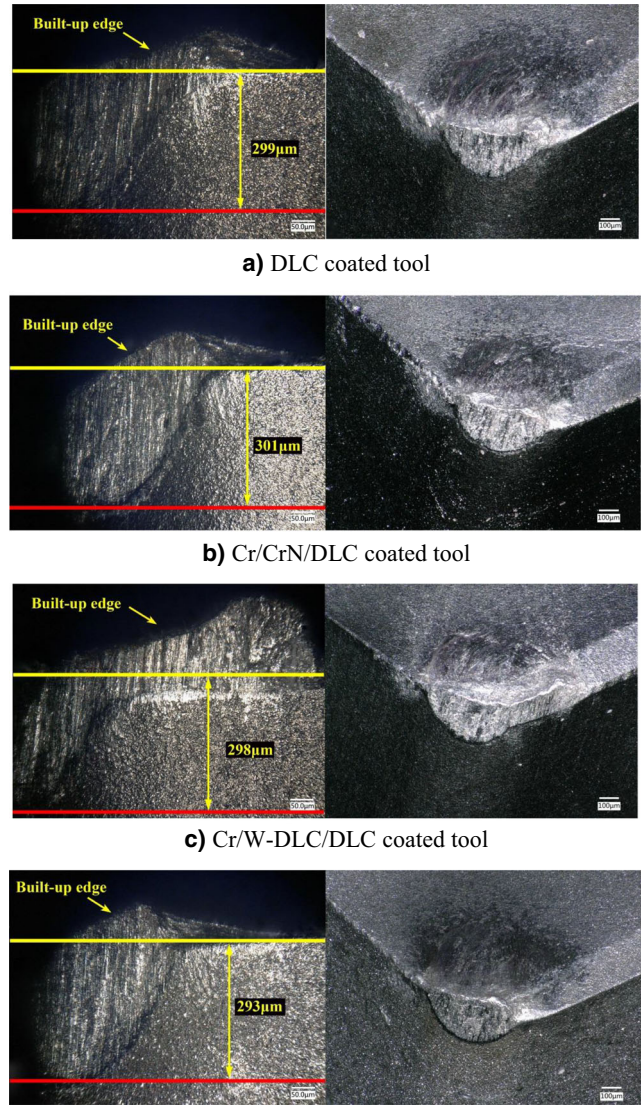

Fig. 14 Wear of uncoated and DLC-coated tools

coated tools and DLC monolayer–coated tools show prolonged tool life of 1.26 times and 1.17 times longer than the uncoated tools, respectively. The tool life of Cr/W-DLC/DLC composite–coated tool was approximately 6200 m, which was 1.35 times longer than that of uncoated tools.

Figure 14 shows the wear morphologies of the tool flank and tool tip on ineffective cutting tools. The main wear form of cutting tools in the machining of Al-Si alloy is boundary wear. The main wear mechanism is adhesion wear and abrasive wear. The high contact pressure and elevated temperature generated during the cutting process can form built-up edge in the tool tip, adhesion then appeared by falling off of built-up edge [34]. In addition, the rake face has many strips of grooves that were formed by mechanical friction of the hard phase in workpiece, as well as the debris exfoliated from built-up edge [35]. The wear of coated tool starts from the damage of the coating. During the cutting process, the coating will show obvious peeling under the influence of mechanical stress and thermal stress. When the coating is peeling off, the chip is in direct contact with the cutting tool substrate, and the temperature of cutting tool is significantly increased. Working at elevated temperature, DLC coating begins to graphitize and the hardness is reduced significantly, which further aggravates the wear of the coated tools.

Surface roughness (Ra) was used to quantitatively characterized the final surface quality on machined surface. The surface roughness is influenced by tool wear and characteristics in the machining process, e.g., the tribological system [36]. In this sense, surface roughness can be employed to determine the cutting performance of cutting tool [37]. Figure 15 shows the difference in the machined surface roughness about DLC-coated and uncoated cutting tools in machining of Al-Si alloy under the same cutting parameters, and the error bars were obtained by standard deviation of the acquired data. As can be seen from Fig. 15, the machined surface roughness generated by DLC-coated tools is significantly lower than that of uncoated tools. This is due to the self-lubricating property of DLC-coated tools, which can reduce the friction coefficient between cutting tool and machined surface [1]. As all known, the low friction coefficients are associated with low workpiece temperature, low tool temperature, and reduction in the tool wear through the cutting processes that can improve the roughness of the machined surface [38]. The investigation results showed the maximum value of surface roughness obtained by DLC monolayer–coated tool and the minimum value of machined surface roughness obtained by Cr/W-DLC/DLC composite–coated tool as among these three kinds of coatings (i.e., DLC, Cr/CrN/DLC, Cr/W-DLC/DLC). It can be induced that the multilayer coating structure can improve the machined surface quality.

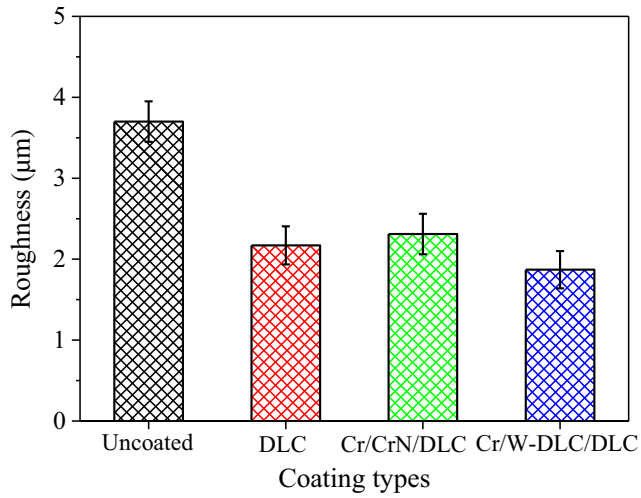

Fig. 15 Surface roughness (Ra) of with different cutting tools

2.4 Comprehensive evaluation of DLC coatings

The comprehensive properties of the DLC-coated tools include mechanical properties and cutting properties, in which various factors such as hardness, toughness, elasticity modulus, internal stress, adhesion, and cutting lives need to be considered. In order to facilitate the intuitive comparative analysis, the comprehensive properties of the three coated tools in this research are shown in Table 5.

The comprehensive evaluation of coating's performance can be carried out by the method of radar chart. Radar chart is a useful graphical display method for displaying multivariate data in a two-dimensional graph. The most obvious feature of radar chart is its intuitive visualization, which allows the status of to-be-evaluated object to be visually displayed [39]. Among the factors affecting the comprehensive properties of DLC-coated cemented carbide tools, hardness, toughness, elastic modulus, adhesion, and cutting lives are beneficial indexes, and the internal stress is a non-profit index. According to the data in Table 5, radar chart is drawn and shown in Fig. 16.

Figure 16 compares the individual indexes: the internal stress, adhesion, and toughness of the Cr/*x*/DLC composite coating were better than the monolayer DLC coating. Among them, Cr/W-DLC/DLC composite coating has the lowest internal stress and the best adhesion and toughness. The tool life of Cr/*x*/DLC composite–coated tools is obviously longer than that of DLC monolayer–coated cemented carbide tool, of which the Cr/W-DLC/DLC composite–coated carbide tools has the longest tool life. Nevertheless, the hardness of the DLC monolayer coating is apparently higher than that of the Cr/*x*/DLC composite coating.

A two-dimensional eigenvector with respect to area and perimeter is formed by the radar chart, and a comprehensive evaluation vector is generated from the two-dimensional eigenvector. The evaluation function results can be obtained according to the comprehensive evaluation vector, as shown in Fig. 17. Considering that the hardness and elastic modulus of Cr/CrN/DLC-coated cemented carbide tools were much lower than that of DLC monolayer–coated cemented carbide tools, so the comprehensive performance is affected. Compared with the comprehensive performance of the DLC-coated cemented carbide tools, the overall performance improvement of Cr/CrN/DLC composite–coated cemented carbide tools is not significant, which is about 1.05 times that of the DLC monolayer–coated cemented carbide tools. The Cr/W-DLC/DLC-coated carbide tools have the best comprehensive performance with 1.35 times that of the DLC monolayer–coated cemented carbide tools.

3 Conclusions

In this research, two types of composite coating with Cr/CrN and Cr/W-DLC transition interlayers and a DLC monolayer coating were prepared on YG8-cemented carbide tools. The influences of different transition interlayers on DLC composite coating's structure, hardness, residual stress, adhesion strength, and cutting characteristics were discussed. The cutting performance of DLC-coated tools was investigated through the cutting tests. The comprehensive performance of DLC coatings was estimated by the method of radar chart. The main conclusions are as follows:

(1) The Cr/*x* transition structure reduces the content of sp^3 covalent bonds in the DLC, which in turn reduces the hardness and elastic modulus of the DLC coating. The

Table 5 Comprehensive properties of the three coated tools

Coating type	DLC	Cr/CrN/DLC	Cr/W-DLC/DLC
Tool life (m)	5400	5800	6200
Hardness (GPa)	20.5	15.23	18.86
Elastic modulus (GPa)	258.76	168.17	180.5
Toughness (N^2)	1168.62	1289.79	1711.72
Adhesion (*N*)	69.68	73.18	116.56
Internal stress (GPa)	0.967	0.379	− 0.021
Machined surface roughness (μm)	2.17	2.31	1.87

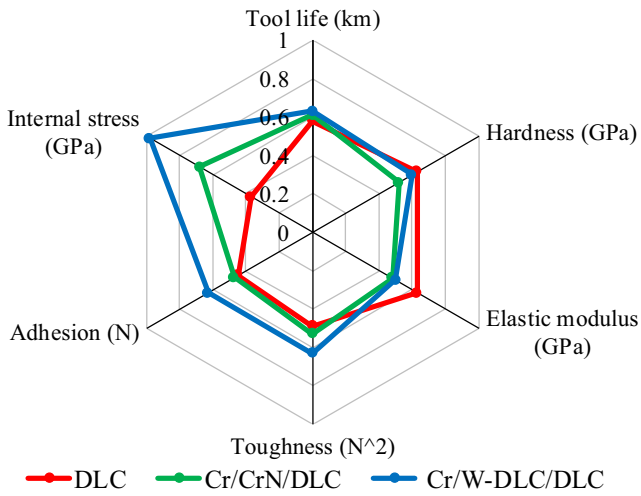

Fig. 16 Comprehensive evaluation of composite coating tools based on Radar chart

sp^3 covalent bond content of composite coatings decreased compare with the monolayer DLC coating, leading to the decrease of hardness and elasticity modulus. However, the transition interlayer contributes to the increase of sp^2 bonds content in the coatings, which can reduce the internal stresses.

(2) The coating/substrate matching performance of the Cr/*x*/*DLC* composite coating is better than the monolayer DLC coating. The Cr/W-DLC/DLC composite coating has the highest adhesion and the highest film toughness, which are 67.28% and 46.47% higher than the DLC monolayer coating respectively. The magnitudes of residual stresses in Cr/W-DLC/DLC and Cr/CrN/DLC composite coatings reduce by 97.83% and 60.81% compared with the monolayer DLC coating, respectively.

(3) Cr/W-DLC/DLC composite–coated tool has the longest tool life in the machining of Al-Si alloys, which is 1.06 times longer than that of Cr/CrN/DLC-coated tool, 1.15 times longer than that of DLC monolayer–coated tool and 1.35 times longer than that of uncoated tool. The adhesion wear and abrasive wear are the main form of cutting tool wear mechanism.

(4) The comprehensive performance of the Cr/W-DLC/DLC composite coating is 1.29 times that of the Cr/CrN/DLC composite coating and 1.35 times that of the monolayer DLC coating.

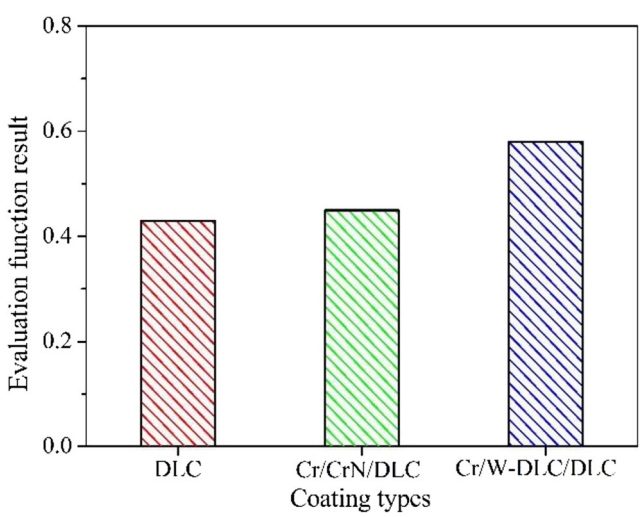

Fig. 17 Evaluation function result of composite coating tools

Funding information This work was financially supported by the National Natural Science Foundation of China (Nos. 51405254, 51676289), the Key Research and Development Plan of Shandong Province (no. 2017GGX203006), a project of Shandong Province Higher Educational Science and Technology Program (no. J18KA026), and the Shandong Natural Science Foundation (no. ZR2017BEE027).

References

1. Baowan P, Saikaew C, Wisitsoraat A (2017) Influence of helix angle on tool performances of TiAlN-and DLC-coated carbide end mills for dry side milling of stainless steel. Int J Adv Manuf Technol 90:3085–3097. https://doi.org/10.1007/s00170-016-9601-5
2. de Paiva JM, Torres RD, Amorim FL, Covelli D, Tauhiduzzaman M, Veldhuis S, Dosbaeva G, Fox-Rabinovich G (2017) Frictional and wear performance of hard coatings during machining of superduplex stainless steel. Int J Adv Manuf Technol 92:423–432. https://doi.org/10.1007/s00170-017-0141-4
3. Bewilogua K, Hofmann D (2014) History of diamond-like carbon films—from first experiments to worldwide applications. Surf Coat Technol 242:214–225. https://doi.org/10.1016/j.surfcoat.2014.01.031
4. dos Santos GR, da Costa DD, Amorim FL, Torres RD (2007) Characterization of DLC thin film and evaluation of machining forces using coated inserts in turning of Al–Si alloys. Surf Coat Technol 202:1029–1033. https://doi.org/10.1016/j.surfcoat.2007.07.100
5. Huang L, Yuan J, Li C (2017) Influence of titanium concentration on mechanical properties and wear resistance to Ti6Al4V of Ti-C: H on cemented carbide. Vacuum 138:1–7. https://doi.org/10.1016/j.vacuum.2017.01.010
6. Huang L, Yuan J, Li C, Hong D (2018) Microstructure, tribological and cutting performance of Ti-DLC/α-C: H multilayer film on cemented carbide. Surf Coat Technol 353:163–170. https://doi.org/10.1016/j.surfcoat.2018.08.076
7. Fukui H, Okida J, Omori N, Moriguchi H, Tsuda K (2004) Cutting performance of DLC coated tools in dry machining aluminum alloys. Surf Coat Technol 187:70–76. https://doi.org/10.1016/j.surfcoat.2004.01.014
8. Ucun I, Aslantas K, Bedir F (2015) The performance of DLC-coated and uncoated ultra-fine carbide tools in micromilling of Inconel 718. Precis Eng 41:135–144. https://doi.org/10.1016/j.precisioneng.2015.01.002
9. Fox-Rabinovich G, Dasch J, Wagg T, Yamamoto K, Veldhuis S, Dosbaeva G, Tauhiduzzaman M (2011) Cutting performance of different coatings during minimum quantity lubrication drilling of aluminum silicon B319 cast alloy. Surf Coat Technol 205:4107–4116. https://doi.org/10.1016/j.surfcoat.2011.03.006
10. Bhowmick S, Alpas A (2008) The performance of hydrogenated and non-hydrogenated diamond-like carbon tool coatings during

the dry drilling of 319 Al. Int J Mach Tool Manu 48:802–814. https://doi.org/10.1016/j.ijmachtools.2007.12.006

11. D'Orazio A, El Mehtedi M, Forcellese A, Nardinocchi A, Simoncini M (2017) Tool wear and hole quality in drilling of CFRP/AA7075 stacks with DLC and nanocomposite TiAlN coated tools. J Manuf Process 30:582–592. https://doi.org/10.1016/j.jmapro.2017.10.019
12. Bhowmick S, Banerji A, Alpas A (2015) Tribological behavior of Al–6.5%,–12%,–18.5% Si alloys during machining using CVD diamond and DLC coated tools. Surf Coat Technol 284:353–364. https://doi.org/10.1016/j.surfcoat.2015.08.073
13. Castillo H, Restrepo-Parra E, Arango-Arango P (2011) Chemical and morphological difference between TiN/DLC and a-C: H/DLC grown by pulsed vacuum arc techniques. Appl Surf Sci 257:2665–2668. https://doi.org/10.1016/j.apsusc.2010.10.039
14. Sheeja D, Tay B, Yu L, Lau S, Sze J, Cheong C (2002) Effect of frequency and pulse width on the properties of ta: C films prepared by FCVA together with substrate pulse biasing. Thin Solid Films 420:62–69. https://doi.org/10.1016/S0040-6090(02)00659-4
15. Huang L, Yuan J, Li C, Wang Z, Zhou T, Yin Z (2016) Influence of annealing temperature on thermal stabilities of hydrogenated amorphous carbon on silicon nitride balls. Vacuum 127:96–102. https://doi.org/10.1016/j.vacuum.2016.02.017
16. Peter S, Günther M, Gordan O, Berg S, Zahn D, Seyller T (2014) Experimental analysis of the thermal annealing of hard a-C: H films. Diam Relat Mater 45:43–57. https://doi.org/10.1016/j.diamond.2014.03.005
17. Yeldose BC, Ramamoorthy B (2008) Characterization of DC magnetron sputtered diamond-like carbon (DLC) nano coating. Int J Adv Manuf Technol 38:705–717. https://doi.org/10.1007/s00170-007-1131-8
18. Duminica F-D, Belchi R, Libralesso L, Mercier D (2018) Investigation of Cr (N)/DLC multilayer coatings elaborated by PVD for high wear resistance and low friction applications. Surf. Coat. Technol 337:396–403. https://doi.org/10.1016/j.surfcoat.2018.01.052
19. Sahoo B, Chattopadhyay A, Chattopadhyay A (2002) Development of diamond coated tool and its performance in machining Al-11% Si alloy. Bull Mater Sci 25:487–491. https://doi.org/10.1007/BF02710534
20. Hong YS, Kwon SH, Tiegang W, Doo-In K, Jihwan C, Kim KH (2011) Effects of Cr interlayer on mechanical and tribological properties of Cr-Al-Si-N nanocomposite coating. T Nonferr Metal Soc 21:s62–s67. https://doi.org/10.1016/S1003-6326(11)61062-5
21. Wu Z, Qi Z, Zhang D, Wei B, Wang Z (2016) Evaluating the influence of adding Nb on microstructure, hardness and oxidation resistance of CrN coating. Surf Coat Technol 289:45–51. https://doi.org/10.1016/j.surfcoat.2016.01.047
22. Hsieh J, Li C, Tan A, Poh C, Tan N (2004) Study of oxidation and wear behaviors of (Nb, Cr) N thin films using Raman spectroscopy. Surf Coat Technol 177:299–305. https://doi.org/10.1016/j.surfcoat.2003.09.008
23. Sharifahmadian O, Mahboubi F (2019) A comparative study of microstructural and tribological properties of N-DLC/DLC double layer and single layer coatings deposited by DC-pulsed PACVD process. Ceram Int 45:7736–7742. https://doi.org/10.1016/j.ceramint.2019.01.076
24. Kurita H, Yamagata H (1998) Effect of hardness on fretting wear characteristics of AC9B and AC8A aluminum alloys. Nippon Kinzoku Gakkaishi 62:50–55. https://doi.org/10.2320/jinstmet1952.62.1_50
25. Wang B, Wang Z, Yin Z, Liu K, Yuan J (2019) Effects of powder preparation and sintering temperature on consolidation of ultrafine WC-8Co tool material produced by spark plasma sintering. Ceram Int 45:19737–19746. https://doi.org/10.1016/j.ceramint.2019.06.227
26. Wang C, Guo B, Shan D, Bai X (2013) Experimental research on micro-deep drawing processes of pure gold thin sheet using DLC-coated female die. Int J Adv Manuf Technol 67:2477–2487. https://doi.org/10.1007/s00170-012-4665-3
27. Sui X, Liu J, Zhang S, Yang J, Hao J (2018) Microstructure, mechanical and tribological characterization of CrN/DLC/Cr-DLC multilayer coating with improved adhesive wear resistance. Appl Surf Sci 439:24–32. https://doi.org/10.1016/j.apsusc.2017.12.266
28. Xu W, Zhou K, Lin S, Dai M, Shi Q, Wei C (2018) Structural properties of hydrogenated Al-doped diamond-like carbon films fabricated by a hybrid plasma system. Diam Relat Mater 87:177–185. https://doi.org/10.1016/j.diamond.2018.06.012
29. Wang C, Cheng L, Liu Y, Zhang H, Wang Y, Shan D, Guo B (2019) Research on micro-deep drawing process of concial part with ultra-thin copper foil using multi-layered DLC film-coated die. Int J Adv Manuf Technol 100:569–575. https://doi.org/10.1007/s00170-018-2757-4
30. Miki Y, Nishimoto A, Sone T, Araki Y (2015) Residual stress measurement in DLC films deposited by PBIID method using Raman microprobe spectroscopy. Surf Coat Technol 283:274–280. https://doi.org/10.1016/j.surfcoat.2015.10.048
31. Zhang S, Sun D, Fu Y, Du H (2004) Effect of sputtering target power on microstructure and mechanical properties of nanocomposite nc-TiN/a-SiNx thin films. Thin Solid Films 447:462–467. https://doi.org/10.1016/S0040-6090(03)01125-8
32. Guo C, Pei Z, Fan D, Gong J, Sun C (2015) Microstructure and tribomechanical properties of (Cr, N)-DLC/DLC multilayer films deposited by a combination of filtered and direct cathodic vacuum arcs. Diam Relat Mater 60:66–74. https://doi.org/10.1016/j.diamond.2015.10.019
33. Escobar C, Caicedo H, Caicedo J (2016) Hafnium and vanadium nitride heterostrutures applied to machining devices. Int J Adv Manuf Technol 82:369–378. https://doi.org/10.1007/s00170-015-7345-2
34. Ahmed YS, Alam MS, Arif AFM, Veldhuis SC (2019) Use of acoustic emission and cutting force signals to monitor built-up edge formation in stainless steel turning. Int J Adv Manuf Technol 103:2257–2276. https://doi.org/10.1007/s00170-019-03607-3
35. Das SR, Panda A, Dhupal D (2017) Experimental investigation of surface roughness, flank wear, chip morphology and cost estimation during machining of hardened AISI 4340 steel with coated carbide insert. Mech Adv Mater Mod Process 3(9):1–14. https://doi.org/10.1186/s40759-017-0025-1
36. Caicedo J, Zambrano O, Aperador W (2018) Improvement of the useful life of the machining tool with the carbonitrides multilayer system. Int J Adv Manuf Technol 96:3263–3277. https://doi.org/10.1007/s00170-018-1826-z
37. Navarro-Devia J, Amaya C, Caicedo J, Martínez J, Aperador W (2019) Hafnium and vanadium nitride multilayer coatings [HfN/VN] n deposited onto HSS cutting tools for dry turning of a low carbon steel: a tribological compatibility case study. Int J Adv Manuf Technol 101:2065–2081. https://doi.org/10.1007/s00170-018-3020-8
38. Davies M, Ueda T, M'saoubi R, Mullany B, Cooke A (2007) On the measurement of temperature in material removal processes. CIRP Ann 56:581–604. https://doi.org/10.1016/j.cirp.2007.10.009
39. Saary MJ (2008) Radar plots: a useful way for presenting multivariate health care data. J Clin Epidemiol 61:311–317. https://doi.org/10.1016/j.jclinepi.2007.04.021

Publisher's note Springer Nature remains neutral with regard to jurisdictional claims in published maps and institutional affiliations.